Numerical study of the initial condition and emission on simulating PM₂.₅ concentrations in Comprehensive Air Quality Model with extensions version 6.1 (CAMx v6.1): Case study of Xi'an

Han Xiao [1], Qizhong Wu [1*], Xiaochun Yang [1,2], Lanning Wang[1], Huaqiong Cheng[1]

[1] College of Global Change and Earth System Science, Beijing Normal University, Beijing 100875, China
[2] Xi'an Meteorological Bureau, Xi'an, Shaanxi Province 710016, China

Correspondence to: Qizhong Wu (wqizhong@bnu.edu.cn)

Abstract. A series of model sensitivity experiments was designed to explore the effects of different initial conditions and emissions in December 2016 in Xi'an, a major city in the "Fen-Wei Plains", which is key area for air pollution control in China. Three methods were applied for the initial condition tests: clean initial simulation, restart simulation, and continuous simulation. In the clean initial simulation test, the sensitivity experiments C00, C06, C12, C18, and C24 were conducted according to the intercepted time periods, and the results showed that the PM₂.₅ model performance was better with the delay of the start time of the intercepted time periods. For experiments C00 to C24, the absolute mean bias (MB) decreased from 51.07 μg/m^3 to 3.72 μg/m^3, and the index of agreement (IOA) increased from 0.49 to 0.86, which illustrates that the model performance of C24 is much better than C00. Sensitivity experiments R1120 and R1124 were used to explore the restart simulation based on the time of the first day of the model simulation. While the start times of the simulations were different, after a spin-up time period, the simulation results with different start times were nearly consistent and the results revealed that the spin-up time was approximately 27 h. For the continuous simulation test, CT12 and CT24 were conducted. The start times of the intercepted time periods for CT12 and R1120 were the same, and the simulation results were almost identical. The simulation results of CT24 performed best in all the sensitivity experiments, with the correlation coefficient (R), MB, and IOA reaching 0.81, 6.29 μg/m^3, and 0.90, respectively. For the emission tests, the updated local emission inventory with construction fugitive dust emissions were added and compared with the simulation results of the original emission inventory. The simulation with the updated local emissions showed a much better performance for PM₂.₅ modelling. Therefore, combining the CT24 method with the updated local emission inventory can satisfactorily improve the PM₂.₅ model performance in Xi'an, and the absolute MB decreased from 35.16 μg/m^3 to 6.29 μg/m^3 and the IOA reached 0.90.

1 Introduction

In recent years, severe air pollution has gradually become a major challenge in China and other developing countries (Wu et al., 2014; Li et al., 2017a). China released a three-year action plan for cleaner air in 2018, and efforts will be focused on areas including the Beijing-Tianjin-Hebei region, the Yangtze River Delta, and the Fen-Wei Plains. As a major city of the "Fen-Wei Plains" key area, Xi'an is located in the Guanzhong Basin. The city is surrounded by the Qinling Mountains to the south, and the Loess Plateau extends to the north and west, which is not conducive to the spread of air pollutants. Xi'an has

suffered severe air pollution in recent years because of its particular topography and rapid economic development (Zhanget al., 2002; Cao et al., 2012). Unfortunately, Xi'an is under the rapid development of urban construction activities with large construction fugitive dust (Long et al., 2016).

35   Air quality modelling systems are an important tool for air pollution assessment and have evolved over three generations since the 1970s, driven by crucial regulations, societal and economic needs, and increasing high-performance computing capacity (Zhang et al., 2012). Various air quality models are widely used in the simulation and forecasting of pollutants, such as the Community Multiscale Air Quality (CMAQ) (Eder and Yu, 2006; Appel et al., 2017), the Comprehensive Air Quality Model with extensions (CAMx) (ENVIRON, 2013), WRF-Chem (Grell et al., 2005), and the Nested Air Quality Prediction

40   Modelling System (GNAQPMS/NAQPMS) (Wang et al., 2006; Chen et al., 2015; Wang et al., 2017). To accurately analyse the apportionment of emission categories and contributions from different source regions for atmospheric pollution, many researchers used the CAMx model with the particulate matter source apportionment technology (PSAT) in different areas of China, including Beijing (Zhang et al., 2018), Tangshan (Li et al., 2013), Pearl River Delta region (Wu et al., 2013), and Yangtze River Delta region (Li et al., 2011). The CAMx showed a satisfactory model performance for the air pollution

45   simulation (Panagiotopoulou et al., 2016).

The input files for the CAMx model include initial/boundary conditions, gridded and elevated point source emissions, and meteorological files (ENVIRON, 2013). Meteorology and emissions inputs can cause high uncertainty for air quality models (Tang et al. 2010; Gilliam et al., 2015). Many researchers have reduced the uncertainty of meteorology through refined physical parameterizations and other techniques, such as data assimilation (Sistla et al., 1996; Seaman, 2000; Gilliam et al., 2015; Li et

50   al., 2019). A reasonable emission inventory is very important for the simulation accuracy of the air quality model. Many researchers have studied East Asian emissions (Kato et al., 1992; Streets et al., 2003; Ohara et al., 2007; Zhang et al., 2009), and tried to construct emission inventories of particulate matter (PM) in China (Wang et al. 2005; Zhang et al. 2006). However, the absence of detailed information on China introduces uncertainty into emission inventories (Cao et al., 2011). In recent years, an increasing number of researchers have focused on constructing and updating regional local emission inventories to

55   improve model performance. Wu et al. (2014) improved the model performance by adding more regional point source emissions and updating the area source emissions in villages and surrounding cities in Beijing. Based on that work, Yang et al. (2019) added local datasets to the emission inventory of the Guanzhong Plain (China), which was applied to simulate $PM_{2.5}$ concentrations using the CMAQ model in Xi'an. Numerous studies have indicated that construction dust emissions play an important role in air pollution, especially in urban areas (Ni et al., 2012; Huang et al., 2014; Wang et al., 2015). In our previous

60   study, we built a particulate matter emission inventory from construction activities at the county level in Xi'an, based on an extensive survey of construction activities and combined with two sets of dust emission factors for a typical city in north China (Xiao et al., 2019).

However, few studies have investigated the initial conditions effects on the simulation or prediction of $PM_{2.5}$ concentrations. Therefore, this study aimed to explore the effects of different initial simulations and emissions on the $PM_{2.5}$ model performance

65   in the CAMx model. A series of model sensitivity experiments for the initial simulation and emissions were designed to find

a suitable method for simulating PM2.5 concentrations with a reasonable initial condition and emission inventory. In addition to Xi'an, other cities may apply a similar research method for simulating PM2.5 concentrations in the future.

The remainder of this paper is organised as follows. Section 2 provides the model descriptions for the WRF-SMOKE-CAMx model system, including meteorological fields, air quality model descriptions, model domain, emission inventory, and processes in Sects 2.1-2.4. Section 3 presents the design of the sensitivity experiments for different initial conditions and emissions. Section 4 discusses the model performance of the initial condition tests and emission tests to simulate the PM2.5 concentration model in Xi'an. The conclusions are presented in Section 5.

2 WRF-SMOKE-CAMx model descriptions

In this study, the National Center for Atmospheric Research (NCAR) Weather Research and Forecasting (WRF v3.9.1.1) model (Skamarock et al., 2008), the Center for Environmental Modeling for Policy Development (CEMPD) Sparse Matrix Operator Kernel Emissions (SMOKE v2.4) (Houyoux and Vukovich, 1999), and the Ramboll Environmental Comprehensive Air Quality Model with Extensions (CAMx v6.1) (ENVIRON, 2013) were used to build up the air quality model system, as shown in Fig.1. The WRF model provided the meteorological conditions for the SMOKE and CAMx models. The SMOKE model was used to process the emissions data and provide 4-D, model-ready gridded emissions for the air quality model CAMx.
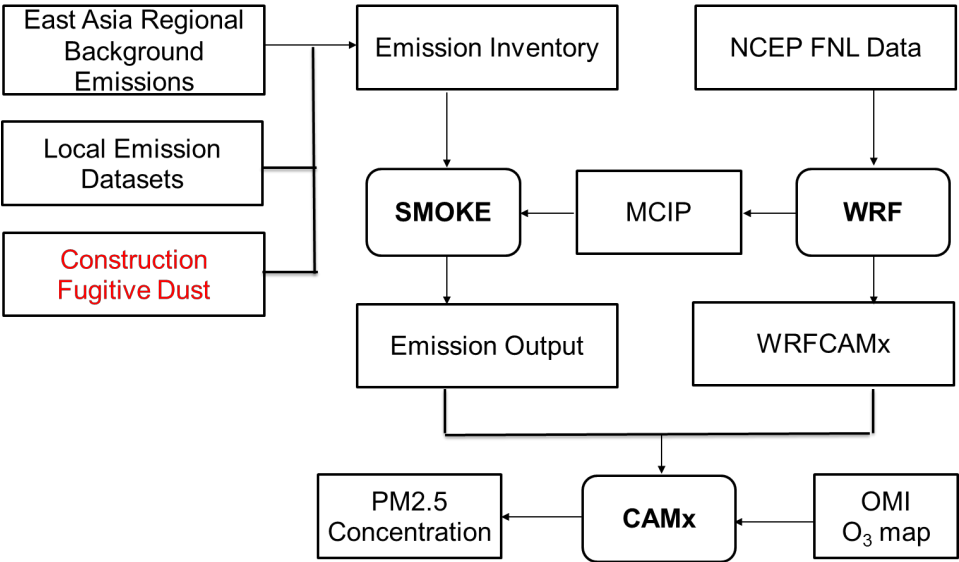
Figure 1. Framework of the WRF-SMOKE-CAMx model system in Xi'an. OMI O₃ map prepares ozone column input files for CAMx to improve the photolysis rate calculation. The CAMx forecasted the air pollutant for the next 48 h.

2.1 Meteorological fields

For the WRF model configuration, we chose the rapid radiative transfer model (RRTM; Mlawer et al., 1997) and Dudhia
for longwave and shortwave radiation options (Dudhia, 1989), WSM3 cloud microphysics (Hong et al., 2004), the YSU scheme
(Hong et al., 2006), the Kain–Fritsch (new Eta) cloud parameterisation (Kain, 2004), and five-layer thermal diffusion scheme
(Dudhia, 1996). The meteorological initial and boundary conditions were derived from the National Centres for Environmental
Prediction (NCEP) global final analysis data (FNL), with a spatial resolution of 1° ×1° and temporal resolution of 6 h. The
simulation was conducted between 20 November 2016 and 20 January 2017.

The simulation effect of daily average temperature (T2) and relative humidity (RH2) simulated by the WRF model in domain
3 were primarily validated by the observation data at 7 monitoring stations in Xi'an, and the station map is shown in Fig. 2.
Some statistical parameters of Appendix A were used to evaluate the model performance and are shown in Table 1, and the
time series is shown in Fig 3. The ME, R, and RMSE of the daily average T2 are 1.37 °C, 0.80, and 1.65 °C, respectively, and
the simulation shows a cooling bias of -0.95 °C. The ME and RMSE of the daily average RH2 are 6.77% and 8.30%,
respectively. The correlation coefficient of the relative humidity is 0.71, which is reasonable. RH2 was slightly overestimated
when the MB was 6.22%.

In previous studies, Yang et al. (2019) used WRF to drive the CMAQ model for winter air quality in Xi'an, and the model
evaluations for winter in 2016 showed that the MB, ME, R, and RMSE of T2 were -2.83 °C, 2.83 °C, 0.89, and 3.29 °C,
respectively. The MB, ME, R, and RMSE of RH2 were 9.59%, 10.63%, 0.71, and 13.43%, respectively. Wu et al. (2010) used
the fifth-generation NCAR/Penn State Mesoscale Model (MM5) as a meteorological driver for the Nested Air Quality
Prediction Modelling System (NAQPMS). The statistical results showed that the MB and R of T2 were 2.1 °C and 0.84, and
those of RH2 were -15.8% and 0.65, respectively. Under the same model configuration and monitoring sites, Yang et al. (2020)
compared the simulated and observed wind speeds at a 10 m altitude (W10) at Xi'an station from 20 November 2016 to 20
January 2017. As the results show, W10 is underestimated. The MB of W10 is -0.14 m/s. The R of W10 is 0.63, indicating a
good agreement between the observations and the model results.

Compared with previous studies, T2 and RH2 have lower MB, ME, and RMSE values. The R of T2 is slightly lower than
in previous studies, while the R of RH2 is higher. Thus, the meteorological simulation in this study is reasonable.
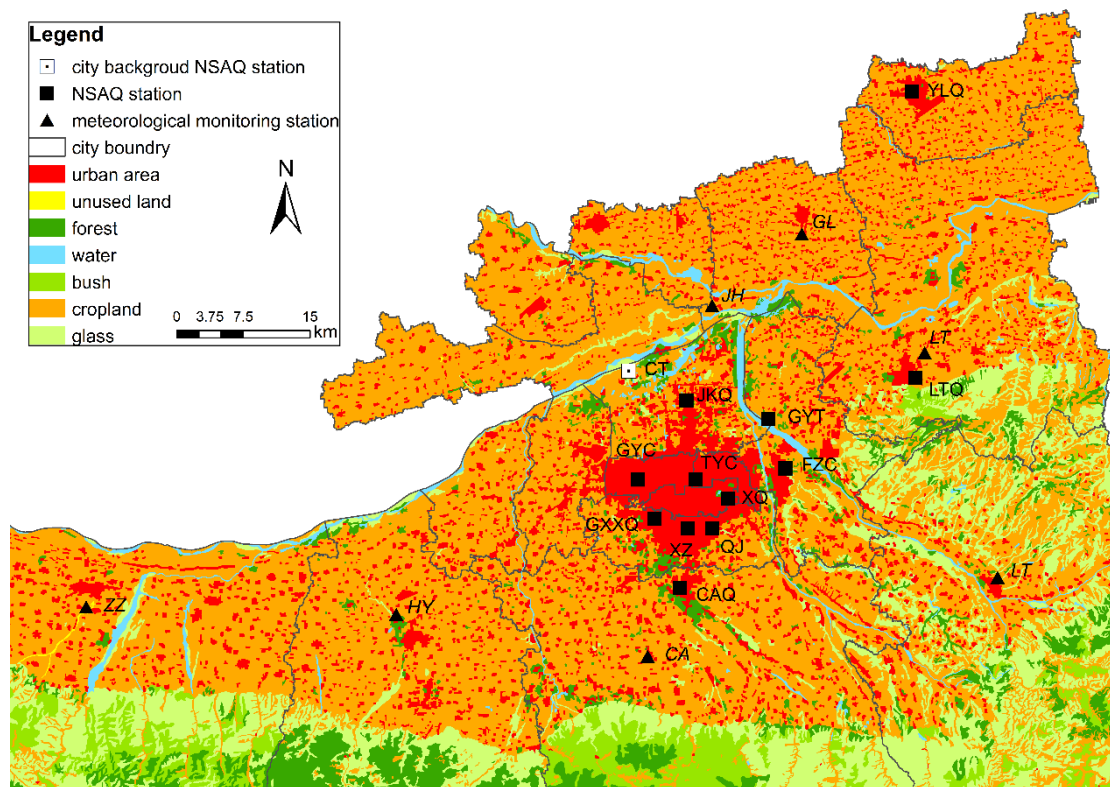
Figure 2. Stations map of the meteorological and air quality monitoring network in Xi'an. The triangles are the meteorological monitoring stations. The square with a dot is the city background station and the black squares are the National Standard Air Quality Observation (NSAQ) Stations: Gaoyachang (GYC), Xingqing (XQ), Fangzhicheng (FZC), Xiaozhai (XZ), Tiyuchang (TYC), Gaoxinxiqu (GXXQ), Jingkaiqu (JKQ), Qujiang (QJ), Gaoyuntan (GYT), Changanqu (CAQ), Yanliangqu (YLQ), Lintongqu (LTQ), and Caotan (CT) Station.
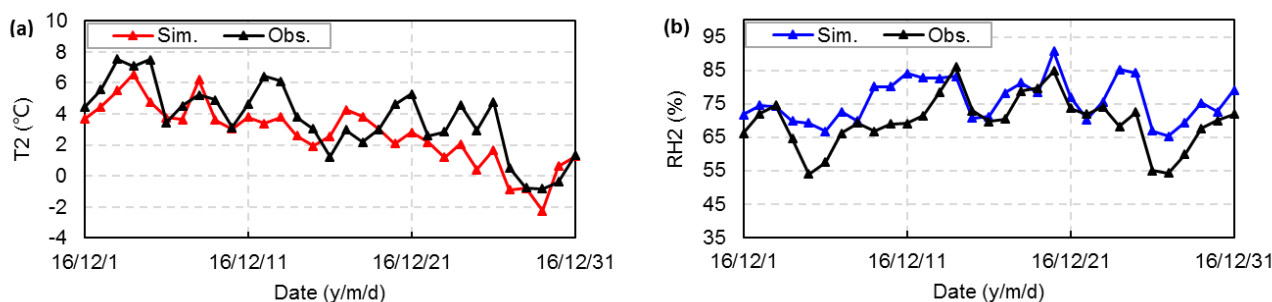
Figure 3. Time series plots of **(a)** daily average simulated and in situ 2 m temperature (T2), and **(b)** simulated and in situ 2 m relative humidity (RH2) at the Xi'an station.

Table 1. Verification statistics of daily temperature at 2 m height (T2), relatively humidity at 2 m height (RH2).

Variable	Mean		ME	MB	R	RMSE
	Obs.	Sim.				
T2(℃)	3.68	2.73	1.37	- 0.95	0.80	1.65
RH2(%)	69.65	75.88	6.77	6.22	0.71	8.30

2.2 Air quality model descriptions

The CAMx model is a state-of-the-science air quality model developed by Ramboll Environ (http://www.camx.com). In this study, the PPM advection scheme (Colella and Woodward, 1984) was used for horizontal diffusion, and the K-theory was selected for vertical diffusion. The Regional Acid Deposition Model (RADM-AQ) (Chang et al., 1987) scheme as the aqueous-phase oxidation, ISORROPIA (Nenes et al., 1999) as the inorganic aerosol thermodynamic equilibrium, and CB05 (Yarwood et al., 2005) as the gas-phase chemical mechanism and the Euler-Backward Iterative (EBI) solver with Hertel's solutions (Hertel et al., 1993) was used in the model system. The resistance model for gases (Zhang et al., 2003) and aerosols (Zhang et al., 2001) in the dry deposition module and the scavenging model for gases and aerosols (Seinfeld and Pandis, 1998) in the wet deposition module was chosen in this study. The CAMx model forecasted the next 48 h of $PM_{2.5}$ concentrations in clean initial simulation testing and is described in Section 2.3. On the first day, CAMx used the results of the ICBCPREP, which can prepare a simple, static CAMx initial condition (IC) and boundary condition (BC). On the following days, it used the different initial conditions of the sensitivity experiments.

2.3 Model domain

Three-nest domains were designed for the WRF model (Fig. 4), with a horizontal resolution of 27 km × 27 km (D1), 9 km × 9 km (D2) 3 km × 3 km (D3). The largest domain (D1) covered most parts of China, the second domain (D2) includes Shaanxi Province, Shanxi Province, Henan Province, and the inner domain (D3), which focused on the 11 cities in the Fen-wei Plain, including Xi'an. The CAMx has only one domain and the settings are the same as those in the D3 domain, while focusing on Xi'an as one sensitivity test area for initial conditions and emissions. To reduce the boundary effects, the CAMx model cuts down the outermost grid of the WRF model and used the variable of the centre grid in the WRFCAMx module. Thus, the CAMx model had three grid cells smaller than the WRF model in the D3 domain. The vertical resolution of WRF was 37 layers from the ground to 5 hPa at the top, and 14 layers were extracted by the WRFCAMx module, which can convert the WRF output files into the data format for the CAMx model.
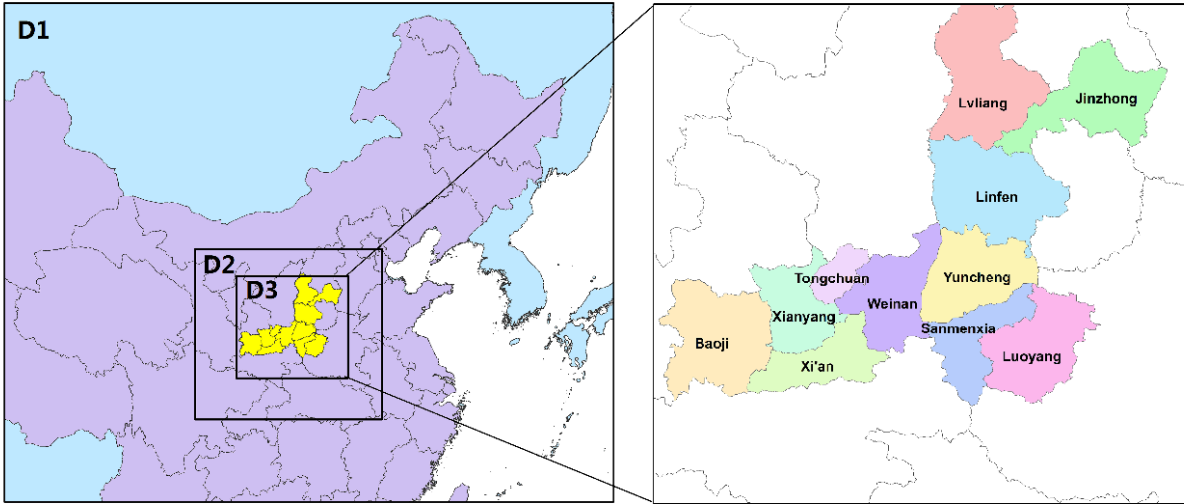
145   **Figure 4.** Three-nest model domain with 27-9-3 km horizontal resolution in the WRF-CAMx modelling system. D1 covers most parts of China, with 148 × 121 grids, and D2 includes Shaanxi, Shanxi and Henan Provinces. The inner domain covers Fen-wei Plain, including Xi'an.

2.4 Emission Inventory and Processes

The SMOKE version 2.4 (Houyoux and Vukovich, 1999) model was used to improve the Fen-wei emissions, especially
150   Xi'an local emissions, and provide gridded emissions for the CAMx model in this study. Based on the emission inventories of a previous study (Yang et al., 2019), this study added the emission quantity of $PM_{2.5}$ from construction fugitive dust in Xi'an to update the local emission inventories. The emission inventories in this study include:

1. The regional emissions in East Asia and the local emissions in the Guanzhong Plain were obtained from Wu et al. (2014) and Yang et al. (2019). Major industrial emissions were slightly adjusted according to the annual report in this study. The
155   emission inventory at the city-level is presented in Table 2.

2. Construction fugitive dust emissions in Xi'an, based on the survey data of construction projects in Fig. 5, were collected in a previous study (Xiao et al., 2019), indicated as a "local area source". This is a new dataset at the county level and updated in 2017. The basic data included the location and area of each construction project. We also replenished the missing construction data and corrected the error information with Google Earth and other geographic information tools to obtain
160   more accurate location information. According to statistics, there were 1595 construction projects in Xi'an in 2017, with 86.1 km^2 of the total construction area. The construction area in the main urban area (Xincheng, Beilin, Lianhu, Yanqiao, Weiyang, and Yanta) was about 62.2 km^2, accounting for 7.5% of the total area in the main urban area. The distribution of the construction fugitive dust emissions in Xi'an is shown in Fig. 6.

We took the statistics-allocation approach to generate gridded area source emissions, which was used to allocate the total
165 emissions to each horizontal model grid according to the related spatial factors. In this study, the Land Scan 2015 Global
Population Database (Dobson et al., 2000) was used as a population spatial factor to allocate the emissions. For the construction
of fugitive dust emissions, we used the area of each construction project as the weight in the surrogate calculation, allocated
the input construction project data to the target polygons (map of administrative division in Xi'an at the county level) based on
the weighted spatial overlap of the input data and target polygons. The spatial results provide the SMOKE model as a spatially
170 allocated factor. The horizontal and vertical allocation of point source emissions were assigned from their longitude-latitude
coordinates and the Briggs algorithm (Briggs, 1972; 1984), respectively. The temporal variation and chemical species
allocation were based on profile files in the SMOKE model.

As shown in Table 2, the NOx emissions ranged from 352.0 kt yr^{-1} to 758.5 kt yr^{-1} between 2008 in Zhang et al. (2009) to
2017 in this study. For PM$_{10}$ emissions in Shaanxi Province, the emissions also increased from 474.0 kt yr^{-1} to 830.0 kt yr^{-1}.
175 The PM$_{10}$ emissions in this study are higher than others because of the construction of fugitive dust. Other emission species,
such as NOx, SO$_2$, NH$_3$, VOCs, and CO, were slightly higher in this study than in previous studies.

Table 2. Emission of major anthropogenic species in Shaanxi Province (Unit: 10^3 tons yr^{-1}).

		CO	NO$_X$	VOCs	NH$_3$	SO$_2$	PM$_{10}$	PM$_{2.5}$
	point source	1196.0	534.4	1572.7	-	724.7	321.7	257.5
	area source	3272.5	224.1	471.9	294.0	490.2	508.3	244.9
	Xi'an	964.1	177.5	370.5	23.4	155.4	198.6	82.8
This study	Baoji	628.3	65.8	256.9	32.8	131.0	68.4	41.1
	Xianyang	773.9	93.2	584.5	25.9	173.0	88.6	66.8
	Tongchuan	80.6	45.0	32.2	4.4	27.5	60.5	32.3
	Weinan	561.9	140.3	500.9	30.5	224.7	132.6	103.7
	Shaanxi Prov.	4468.5	758.5	2044.6	294.0	1214.8	830.0	502.3
Zhang et al. 2009	Shaanxi Prov.	3528.0	352.0	491.0	-	907.0	474.0	328.0
CCCPSC, 2011	Shaanxi Prov.	-	521.2	-	-	938.7	580.1	-
Yang et al. 2019	Shaanxi Prov.	4369.0	736.9	1994.1	293.2	1193.7	770.4	534.9
Yang et al. 2020	Shaanxi Prov.	3905.8	575.7	1904.3	287.6	802.3	564.0	398.1
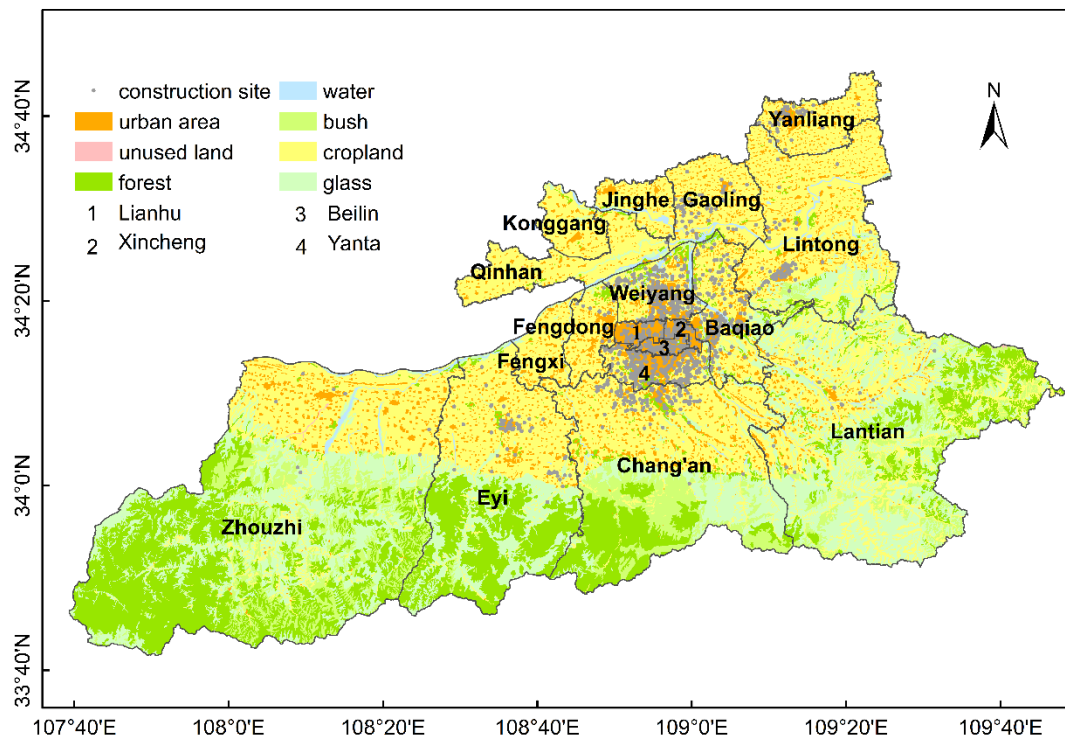
Figure 5. Spatial distribution of construction sites in Xi'an. Gray dots indicate the construction sites. The base map shows the types of land use (Xiao et al., 2019).
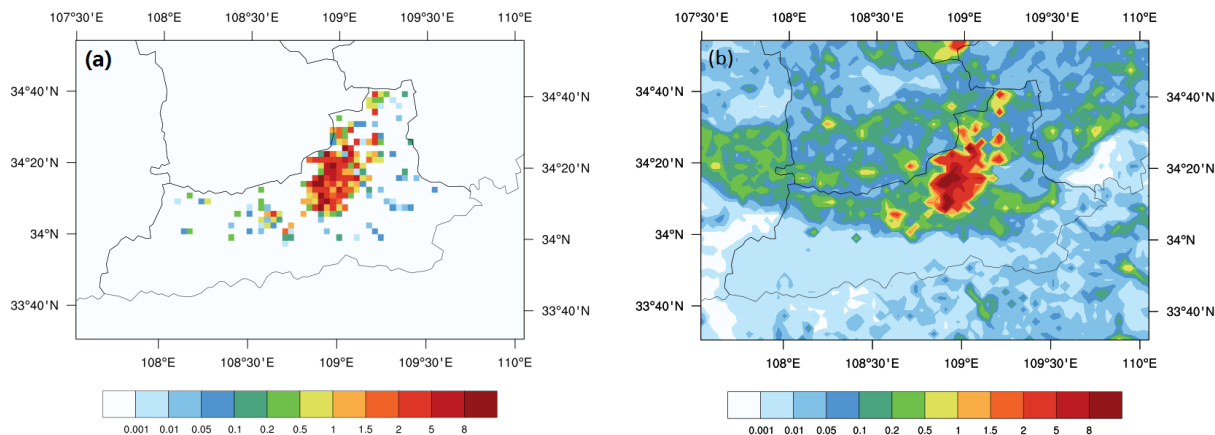
Figure 6. Spatial distribution of PM_{10} emissions in Xi'an and its surrounding area. (a) only construction fugitive dust in Xi'an. (b) all surface PM_{10} emissions in Xi'an. The grid size is 3 km x 3 km. Unit: $g/km^2 \cdot s$

3 Sensitivity experiments design

A set of model sensitivity experiments under different initial conditions and emissions were designed in this study. Three methods were applied for the initial condition tests: using the clean initial condition files as clean initial simulation, using the restart files as restart simulation and the continuous simulation. For the emission tests, we compared the simulation results of the original emission inventory and the updated local emission inventory with construction fugitive dust emissions. The configurations of the simulation sensitivity experiments are shown in Table 3, and the time period for each initial condition experiment is shown in Fig. 7.

3.1 ICON test for using the clean initial condition files

The icbcprep module used a clean-troposphere vertical profile to generate the initial concentration fields for each day of the simulation to use the clean initial condition files. The output files of CAMx were initialised at 13:00 UTC. The CAMx model forecasted the next 48 h of $PM_{2.5}$ concentrations in each cycle simulation. By extracting data from simulated results based on different time periods (0–24 h, 6–30 h, 12–36 h, 18–42 h and 24–48 h, respectively) shown in Fig. 7 (a), we conducted sensitivity experiments C00, C06, C12, C18, and C24, and explored the influence of different time periods on the simulation effect of $PM_{2.5}$. For the sensitivity experiment C00, the data of the period for the first 24 h of the output file were cut and merged for analysis. For C06, the first 6 h of data was spin-up time; we cut and merged the data from 19:00 UTC to 18:00 UTC on the second day. C12, C18, and C24 used the same method to extract and merge data, and their spin-up times were the first 12 h, 18 h, and 24 h of data, respectively.

3.2 ICON test for using the restart files

The meteorological data for the period 12–36 h were cut to estimate the $PM_{2.5}$ concentrations by restarting the simulation of the CAMx model. The icbcprep module also used clean initial concentration fields at the beginning of the first-day simulation to use the restart files. The gridded three-dimensional instantaneous concentrations of all species on all grids were written at the end of the simulation to allow for a model restart. Then, ICON used the 24-h forecast results from the day before as the initial conditions for the following days, as shown in Fig. 7 (b). The first day of the simulation started at 12:00 UTC, and the following days started at 00:00 UTC. To explore how long the spin-up time can eliminate the error caused by the initial value, the sensitivity experiments R1120 and R1124 were set at the time of the first day for the model simulation, which began on the 20th and 24th of November 2016, respectively.

3.3 ICON test for continuous simulation

For the continuous simulation, sensitivity experiments CT12 and CT24 were at the start time of the intercepted time periods, which started at 00:00 UTC and 12:00 UTC, respectively, as shown in Fig. 7 (c). For CT12, the meteorological data of the period 12–36 h were cut and merged into one file. The 24–48 h period was cut and merged for CT24. We also built the

continuous emission files using the SMOKE model. During the simulation, there was no interruption, and finally, a long-term sequence simulation result for each start time was generated.

3.4 Emission test for different emission inventories

Based on the initial condition tests, we selected the best method to perform the emission sensitivity experiments. We 220 compared the simulation results of the original emission inventory (sensitivity experiments Enc) and the updated local emission inventory with the construction fugitive dust emissions (sensitivity experiments Ec) for the emission tests.

Table 3. The simulation experiment configurations. C00-C24, R1120, R1124, CT12 and CT24 were used to investigate the impact of simulation methods, start time and extracted time period. The impact of different emission inventory was investigated 225 by Ec and Enc. Method C, R, CT presented for the clean initial condition simulation methods, restart simulation and continuous simulation. Emission inventory nc and c presented for the original emission inventory and the updated local emission inventory with the construction fugitive dust emissions, respectively.

Experiment	Method	Emission inventory	Start time and extracted time period
C00	C	c	2016/11/26 0-24th hour
C06	C	c	2016/11/26 6-30th hour
C12	C	c	2016/11/26 12-36th hour
C18	C	c	2016/11/26 18-42th hour
C24	C	c	2016/11/26 24-48th hour
R1120	R	c	2016/11/20 12-36th hour
R1124	R	c	2016/11/24 12-36th hour
CT12	CT	c	2016/11/26 12-36th hour
CT24/Ec	CT	c	2016/11/26 24-48th hour
CT24/Enc	CT	nc	2016/11/26 24-48th hour
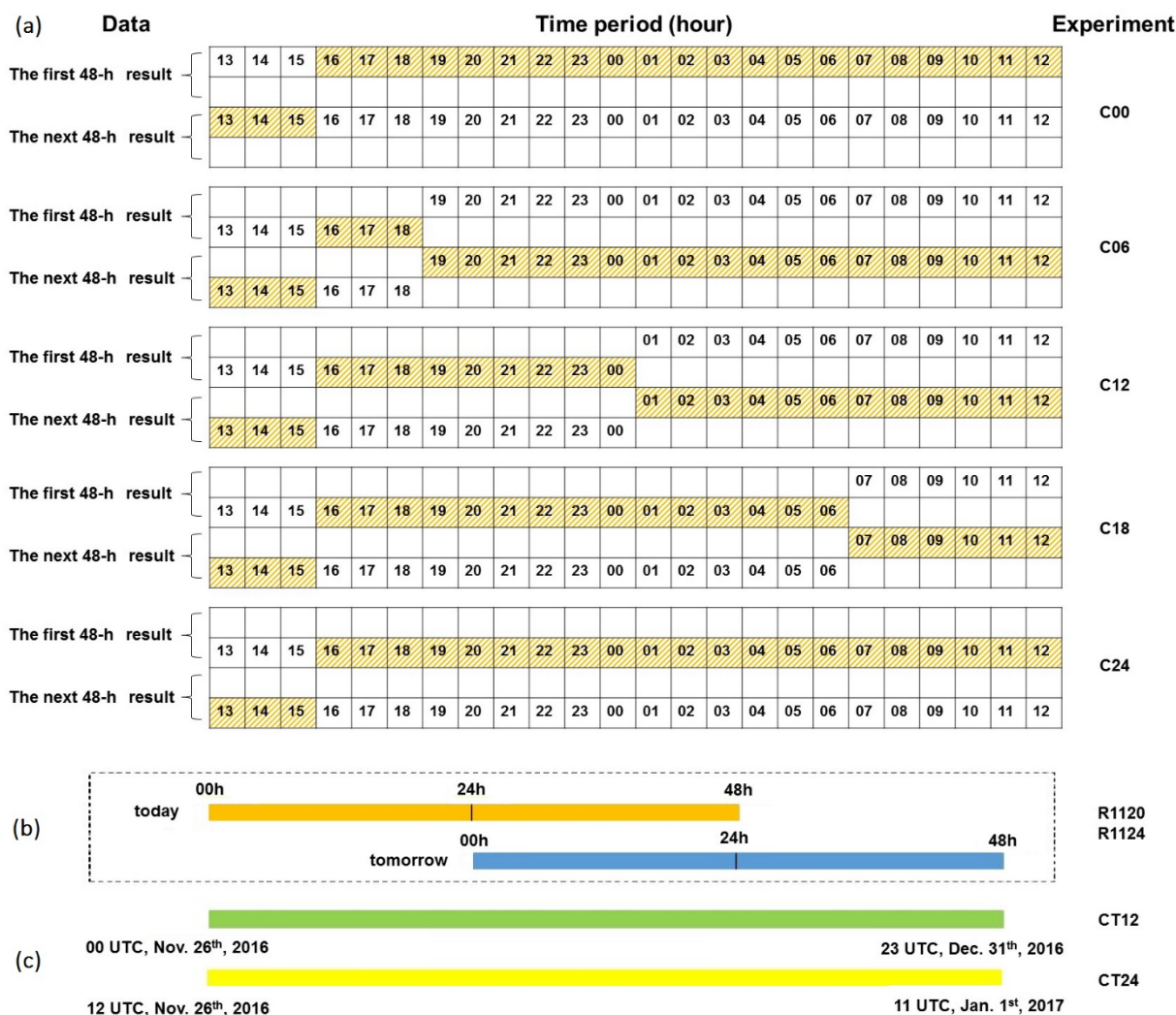
Figure 7. Time period for each initial condition experiments. **(a)** shows the time period for Clean initial condition (mark C) experiments. The output files of CAMx were initialised at 13:00 UTC every day and the CAMx model forecasted the next 48 hours' $PM_{2.5}$ concentrations in each cycle simulation. The sensitivity experiments C00, C06, C12, C18, and C24 extract different time periods (0–24 h, 6–30 h, 12–36 h, 18–42 h and 24–48 h, respectively) in each output file as valid data, represented by the grids with a number. Each grid represents an hour and the numbers on the grids indicate the hours of the data. The grids with numbers represent the valid time period for each output file. The 24-hour data of a day is cut and merged from 16:00 UTC in the valid time period of each output file to analyse from 0:00 Beijing time (16:00 UTC) every day. The shaded grids represent the data for one single day. **(b)** shows the time period for Restart (mark R) experiments. The meteorological data of the 12–36 h period was extracted to estimate the $PM_{2.5}$ concentrations by restart simulation. The first day of the simulation

starts at 12:00 UTC, and the following days starts at 00:00 UTC. **(c)** shows the time period for continuous simulation (mark
CT) experiments. The meteorological data of the 12–36 h period is cut and merged to one file for CT12 and the period 24–48
h was cut and merged for CT24.

4 Results and discussion

In this study, we collected the observations in December 2016 and evaluated the model performance and improvement.
Hence, the model ability from both the meteorological field and daily $PM_{2.5}$ simulations in Xi'an was evaluated.

4.1 Model performance of the initial condition tests

There are 13 NSAQ Stations in Xi'an, which are marked as squares in Fig 2. Nine stations are in urban Xi'an, including
GYC, XQ, FZC, XZ, TYC, GXXQ, JKQ, QJ, and GYT. Three stations are located in suburban towns, including CAQ, YLQ,
and LTQ. The CT Station is the city background station, which is located in northern urban Xi'an.

4.1.1 Sensitivity experiments for using clean initial condition files

A Taylor nomogram (Taylor, 2001; Gates et al., 1999) was used to evaluate the accuracy of simulated $PM_{2.5}$ daily
concentrations for NSAQ stations, which was used for the sensitivity experiments of using the clean initial condition files, as
shown in Fig 8. There are three statistical parameters to evaluate model accuracy: the correlation coefficient (R), normalised
standard deviation (NSD), normalised root, and mean square error (NRMSE) in Taylor nomogram (Taylor, 2001; Gates et al.,
1999; Chang et al., 2004). The sensitivity experiments C00, C06, C12, C18, and C24 are shown by symbols of different colours.
We randomly selected 3 stations in urban Xi'an, 2 stations in county towns, and a background station to show the simulation
results. And the "AVG" meant the average of 13 NSAQ Stations.

As shown in Fig 8, R is 0.36–0.76 for the sensitivity experiments C00, C06, C12, C18, and C24. C24's R is the largest and
best for all NSAQ Stations, and C00's is the lowest. The NRMSE, which measures the distance from the marker to the REF
in the Taylor nomogram, is smallest and best for C24, and longest for C00. For NSD, most NSAQ Stations have similar
regularity, that is, the NSD values from C00 to C24 are getting closer to "1". The other statistical parameters are presented in
Table 4. From experiments C00 to C24, the absolute mean bias (MB) and the mean error (ME) decreased from 51.07 µg/m^3 to
3.72 µg/m^3 and from 74.09 µg/m^3 to 45.82 µg/m^3, respectively. The absolute normal mean bias (NMB) and the normal mean
error (NME) decreased from 29.73% to 2.17% and from 43.12% to 26.67%, respectively. The index of agreement (IOA)
increased from 0.50 to 0.8. In general, the C24 model performance is better than that of other sensitivity experiments in clean
initial simulation tests.
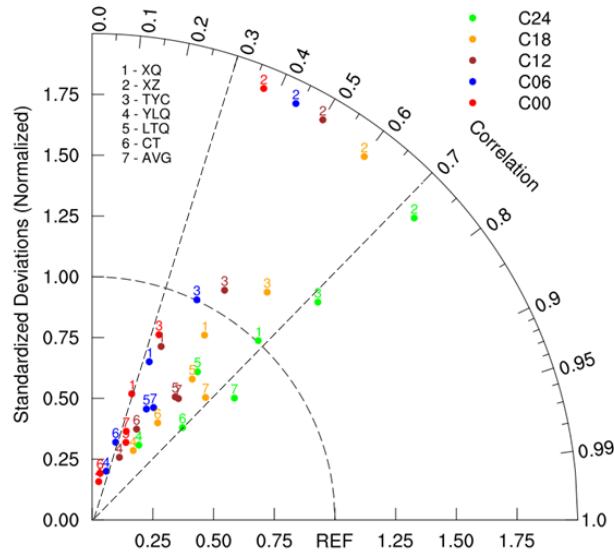
Figure 8. Taylor nomogram for modelled and observed daily averaged PM$_{2.5}$ concentrations for the sensitivity experiment using the clean initial condition files. The "AVG" refers to the average of 13 NSAQ Stations. The sensitivity experiments C00, C06, C12, C18, and C24 are represented using symbols of different colours. According to Chang et al. (2004) REF represents a perfect simulated result for the air quality model.

4.1.2 Sensitivity experiments for using restart files

Sensitivity experiments R1120 and R1124 were set at the time of the first day for the model simulation to explore the restart simulation. Starting from 12:00 UTC on the 24th of November, the PM$_{2.5}$ concentration simulation results of the two sensitive experiments, R1120 and R1124, are shown in Fig 9. At first, the results of the two sensitivity experiments were very different, and then the two lines were gradually fitted until 16:00 UTC on November 25th. After 16:00 UTC on the 25th of November, the two lines fitted almost completely. Therefore, a spin-up time of 27 h can eliminate the error brought by the initial field for the PM$_{2.5}$ concentrations in the CAMx model.

As shown in Table 4, the model performances of the sensitivity experiments R1120 and R1124 are similar in December 2016. For the sensitivity experiments R1120 and R1124, the R value between observations and simulations was 0.70. The mean bias (MB) and mean error (ME) were 4.01 μg/m^3 and 49.68 μg/m^3, respectively. The normal mean bias (NMB) and normal mean error (NME) were 2.33% and 28.92%, respectively. The root mean square error (RMSE) was 67.28, and the IOA reached 0.82.
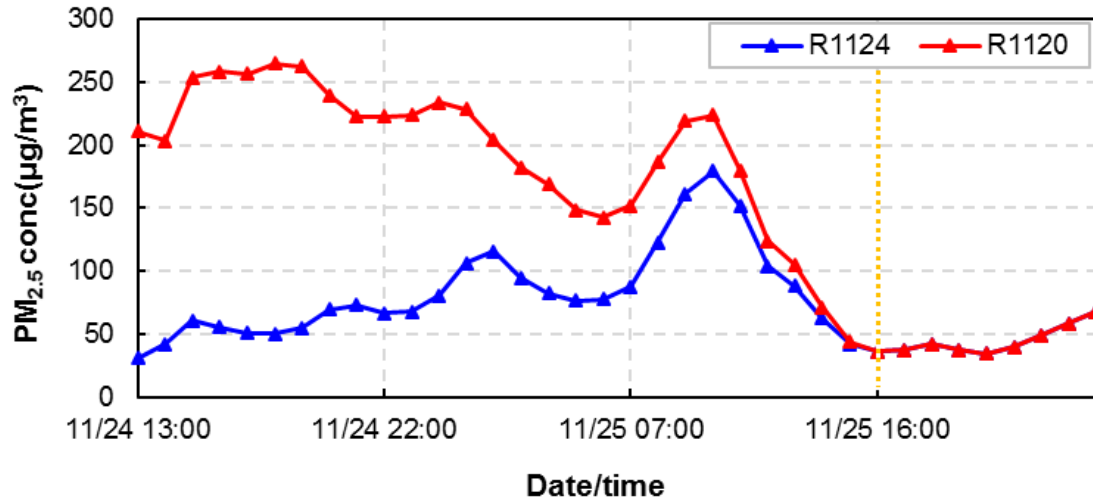
Figure 9. The time series of hourly simulated PM$_{2.5}$ concentrations using the restart files during a spin-up time period. The red
285   and blue lines represent the model sensitivity experiments R1120 and R1124, respectively. The starting day of the model
simulation for R1120 was 20th November 2016, and for R1124 was 24th November 2016.

4.1.3 Sensitivity experiments for continuous simulation

For the continuous simulation, sensitivity experiments with CT12 and CT24 were conducted. Although the sensitivity
experiments CT12 and R1120 use different methods to generate the initial concentration fields, the start times of the intercepted
290   time periods for the two experiments were the same. The PM$_{2.5}$ concentrations of CT12 and R1120 are presented in Fig 10. As
shown in Fig 10, the points lie very close to the perfect line "y=x", which indicates that the simulation results of CT12 and
R1120 were nearly identical.

The model starting time of sensitivity experiments CT12 and CT24 are 26th November at 00:00 UTC and 26th November at
12:00 UTC, respectively. The concentration accumulation of CT24 was 12 h higher than that of CT12. As shown in Fig 11,
295   there is an air pollution peak in December 2016, in which CT24 matches better than CT12. The statistical parameters of CT12
and CT24 are presented in Table 4. The mean bias (MB) and mean error (ME) of CT24 results were 6.29 μg/m^3 and 42.67
μg/m^3, respectively, which are slightly better than the CT12 results. The root mean square error (RMSE) of the CT24 results
is 68.21, which is also slightly better than the CT12 results. From CT12 to CT24, the R and IOA increased from 0.69 to 0.81
and from 0.81 to 0.90, respectively. Thus, the sensitivity experiments with CT24 have better model performance than CT12.

300
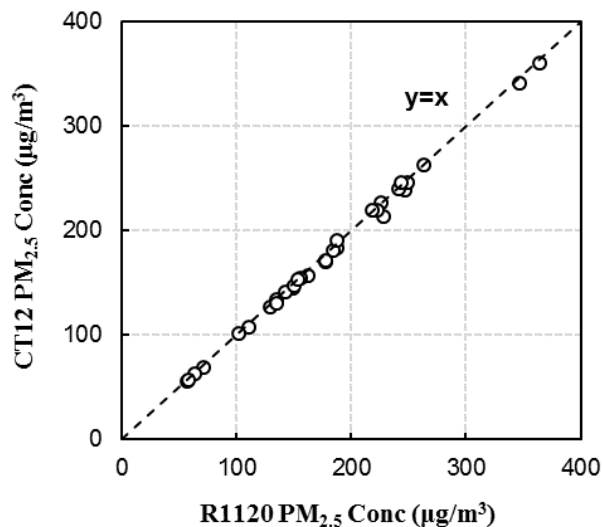
Figure 10. Scatter diagram of the R1120 and CT12 experiments of PM$_{2.5}$ concentrations. Line "y=x" represents the simulated of R1120 is the same to CT12.
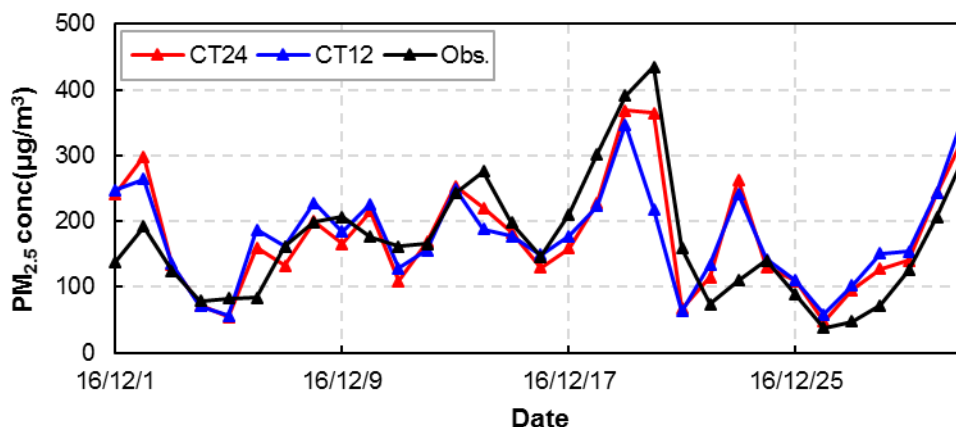
Figure 11. Time series of daily PM$_{2.5}$ concentrations for continuous simulation in Xi'an. The black line represents observations,

305 the blue and red lines show simulated data started at November 26th 00:00UTC and November 26th 12:00UTC, respectively.

4.2 Model performance of emission tests

The Taylor nomogram for modelled and observed daily averaged PM$_{2.5}$ concentrations for all initial condition sensitivity experiments, as shown in Fig 13. The red symbols indicate the sensitivity experiment to use the clean initial condition files, the blue symbols represent the sensitivity experiment to use the restart files, and the brown symbols show the sensitivity

310 experiment for continuous simulation. One experiment per symbol. The circles and triangles represent the "bias". As shown in Fig. 13, R is 0.36–0.81 in all initial condition sensitivity experiments. The CT24 R value is the highest in all initial condition sensitivity experiments. The CT24 marker has the shortest distance to the "REF" than other initial condition sensitivity experiments, which means that the NRMSE is the smallest. The NSD of CT24 is 0.92, which shows that the modelled and observed patterns have a more consistent variation amplitude. According to these statistical parameters, the sensitivity

315 experiments CT24 have the best model performance compared to other initial condition sensitivity experiments.

Based on the initial condition tests, we selected the best method, CT24, to perform the emission sensitivity experiments, as shown in Fig 12. CT24 is the experiment with construction fugitive dust emissions (sensitivity experiments Ec), and the sensitivity experiments Enc is not. As shown in Fig. 12, the simulated PM$_{2.5}$ concentrations of Ec exhibited a better model performance than that of Enc in the high concentration range. As shown in Fig. 13, the R values of Ec and Enc are 0.81 and

320 0.85, respectively. The NRMSE for Enc is smaller than Ec, as shown in the Taylor nomogram. However, the NSD of Ec, 0.92, is better than that of Enc, 0.74. Moreover, the bias of Enc is much larger than that of Ec. The other statistical parameters are presented in Table 4. The ME decreased from 49.18 μg/m^3 to 42.67 μg/m^3 and the IOA of simulation results with the updated local emissions was 0.90. Thus, compared to the simulation results based on the original emission inventory, the new simulation results, driven by the updated local emissions, showed an improved performance on PM$_{2.5}$ concentrations.
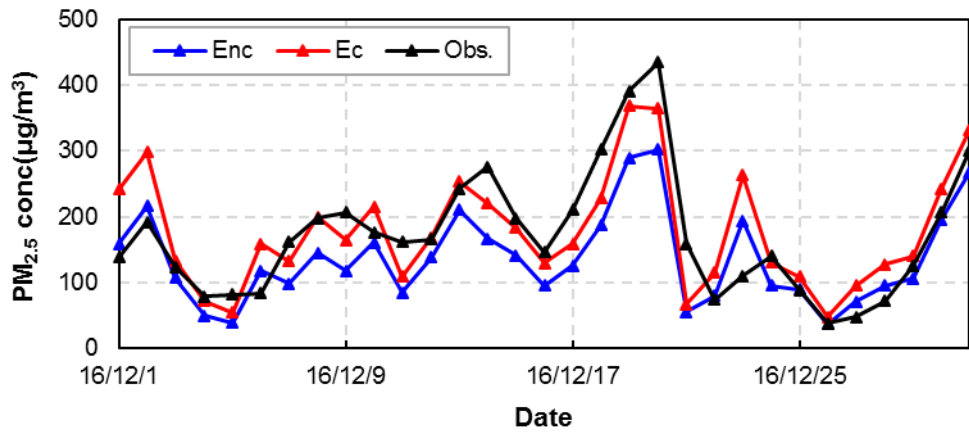
325

Figure 12. Time series of daily observed and simulated PM$_{2.5}$ concentrations averaged from 13 NSAQ Observation Stations during December 2016 in Xi'an. The black line represents the observations, the blue line represents the simulated values by the CAMx model with construction fugitive dust, and the red line represents the simulated values without construction fugitive dust.

330
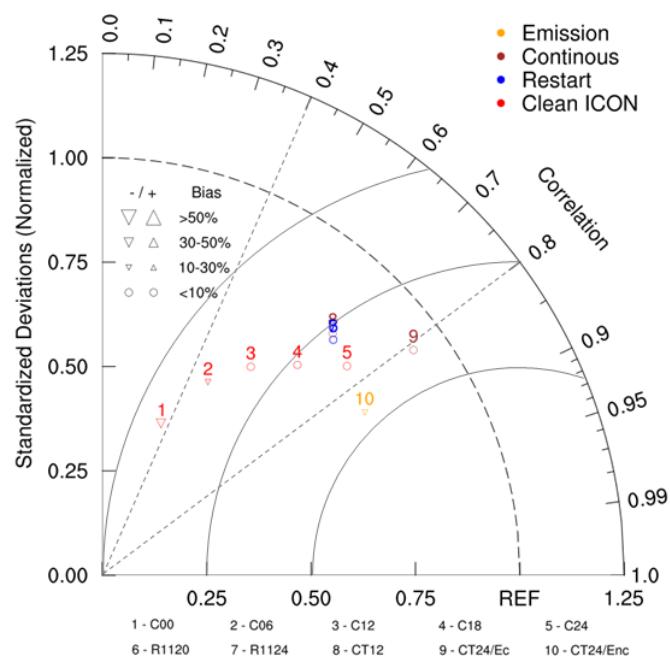
Figure 13. Taylor nomogram for modelled and observed daily PM$_{2.5}$ concentrations for all sensitivity experiments under different initial conditions and emissions. The red symbols indicate the clean initial simulation, the blue symbols represent the restart simulation, the brown symbols show the sensitivity experiment for continuous simulation, and the orange symbols are for emission tests. The triangles and circles signify "Bias". The scale of the triangle's size represents the bias value, and the direction of the triangle's vertex represents positive or negative.

Table 4. Statistical measures of the modelled daily PM$_{2.5}$ in Xi'an, unit: μg/m³.

	R	MB(μg/m³)	ME(μg/m³)	NMB%	NME%	RMSE	IOA
C00	0.36	-51.07	74.09	-29.73	43.12	100.72	0.49
C06	0.48	-24.17	60.95	-14.07	35.48	85.50	0.61
C12	0.58	-12.88	53.25	-7.50	30.99	76.64	0.70
C18	0.68	-7.00	48.83	-4.08	28.42	68.85	0.78
C24	0.76	-3.72	45.82	-2.17	26.67	60.12	0.86
R1120	0.70	4.01	49.68	2.33	28.92	67.28	0.82
R1124	0.70	4.01	49.68	2.33	28.92	67.28	0.82
CT12	0.69	6.73	50.20	3.92	29.22	68.21	0.81
CT24/Ec	0.81	6.29	42.67	3.66	24.83	55.29	0.90
CT24/Enc	0.85	-35.16	49.18	-20.47	28.63	61.22	0.86

4.3 Model performance of SO₂ and NO₂

Sulfur dioxide (SO_2) and nitrogen dioxide (NO_2) concentrations are important precursors of SO_4 and NO_3, which are particulate matter components. Daily observed and simulated SO_2 and NO_2 concentrations averaged from 13 NSAQ Observation Stations under the initial restart simulation. Figure 14 shows the time series of daily average SO_2 and NO_2 concentrations from 13 NSAQ Observation Stations under the initial restart simulation, and the statistical results are listed in Table 5. The model has an evident overestimation of SO_2, with an average bias of 156.31 μg/m³, and the observed SO_2 concentration was only 18% of the simulated value. The main reason is that the implementation of desulfurization projects for important emission sources, such as coal-fired power plants, has not been fully considered, which has led to an overestimation of SO_2 emissions in the emission inventory. Li et al. (2017b) found that the SO_2 emissions in China decreased by 75% from 2007 to 2016, i.e. SO_2 emissions in 2016 were about 25% in 2007. In addition, the intensity of emissions reduction has uneven spatial distribution. The model performance of the NO_2 concentration is better, the IOA is 0.82, and the MB is only 3.32 μg/m³. There is a high consistency of the variation trend between the simulated and observed SO_2 and NO_2 concentrations, with R being 0.81 and 0.75, respectively.
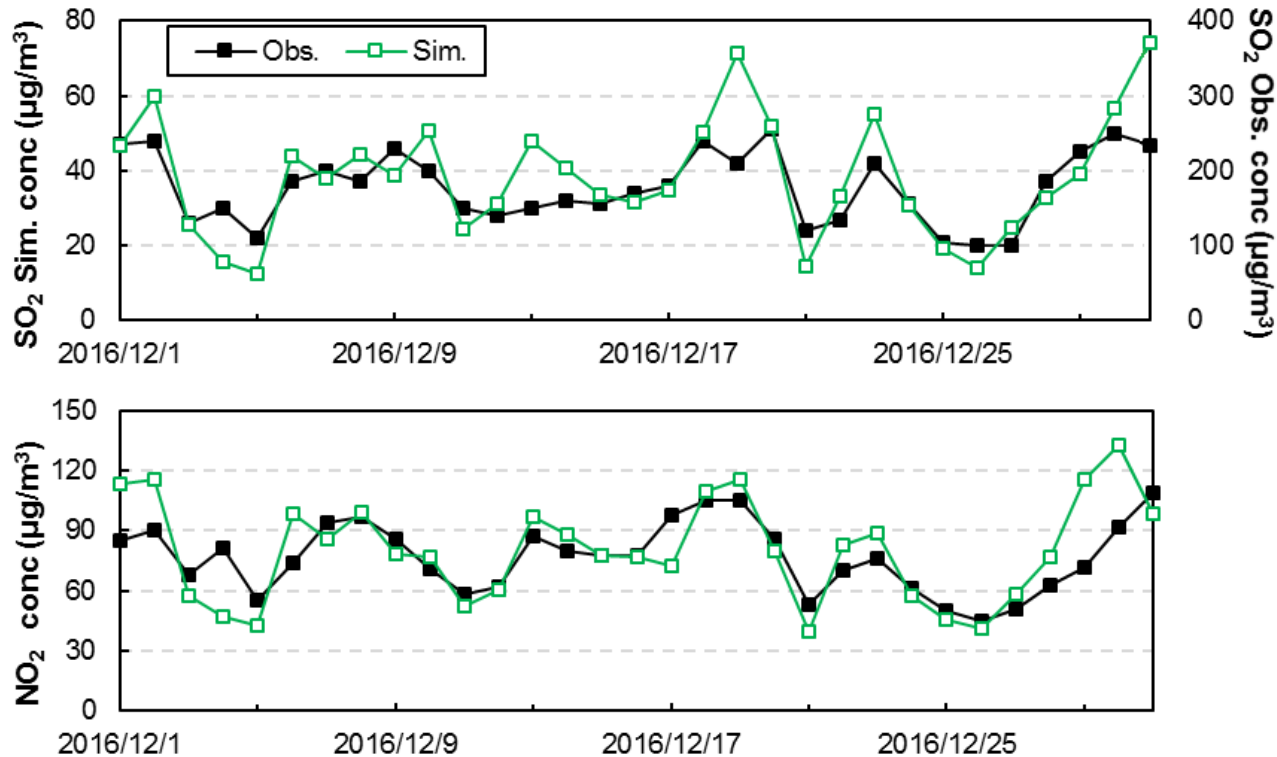
Figure 14. Time series of daily observed and simulated SO_2 (top) and NO_2 (bottom) concentrations averaged from 13 NSAQ Observation Stations during December 2016 in Xi'an. The black and green lines indicate observed and simulated results, respectively.

Table 5. Statistical verification parameters of SO_2 and NO_2 during December 2016 in Xi'an.

Species	Mean($\mu g/m^3$)		R	MB	ME	NMB	NME	RMSE	IOA
	Obs.	Sim.		($\mu g/m^3$)	($\mu g/m^3$)				
SO_2	35.45	191.76	0.81	156.31	156.31	4.41	4.41	171.73	0.11
NO_2	76.77	80.09	0.75	3.32	12.86	0.04	0.17	17.13	0.82

4 Conclusions

The WRF-SMOKE-CAMx model system was used to simulate fine particulate matter ($PM_{2.5}$) concentrations in Xi'an in December 2016. In this study, the construction fugitive dust emissions in Xi'an were added to the SMOKE model to update the local emission inventory. A series of model sensitivity experiments for the initial conditions and emissions were designed to improve the model performance in the megacity, Xi'an.

Three methods were applied for the initial condition tests: using the clean initial condition files as clean initial simulation, using the restart files as restart simulation and continuous simulation. The updated emission inventories drive all initial condition sensitivity experiments. The emission tests are based on the initial condition sensitivity experiment, which has the best model performance.

Comparing the model performance of $PM_{2.5}$ concentrations in different model sensitivity experiments in Xi'an, we found that the model combining the continuous simulation method with the updated local emission inventory can effectively improve the model performance. According to statistical parameters, for initial condition tests, the model performances of CT24, C24, and R1120/R1124 are the best. R ranges from 0.36 to 0.81 in all initial condition sensitivity experiments. The R value of CT24 is the largest and best in all initial condition sensitivity experiments. The R values of C24 and R1120/R1124 can reach 0.76, 0.70, respectively. The MB of CT24, C24 and R1120/R1124 are lower, which are 6.29 $\mu g/m^3$, -3.72 $\mu g/m^3$ and 4.01 $\mu g/m^3$, respectively. The IOA of CT24, C24, and R1120/R1124 reached above 0.8, of which CT24 was 0.9. Compared with other methods, the method of using the clean initial condition files has a longer simulation time and larger data volume. Therefore, the method of continuous simulation for hindcasts, which is to retrieve $PM_{2.5}$ concentrations, is suggested. For air quality forecasting, we can prioritise the method of restart simulation. In addition, for simulating $PM_{2.5}$ concentrations using the CAMx model, the simulation requires a spin-up time of at least 27 hours. This can improve the simulation effect and reduce the simulation time.

This study updated the emissions inventory, which added construction fugitive dust emissions to the original emissions inventory. Compared to the simulation results based on the original emission inventory, the new simulation results, which were driven by the updated local emissions, showed a much better performance in $PM_{2.5}$ modelling. The absolute MB decreased

from 35.16 µg/m^3 to 6.29 µg/m^3 and the IOA of simulation results with the updated local emissions was 0.90. Therefore, the right addition of emissions will also help to improve the effects of simulation and forecasting.

Finally, we recommend the continuous simulation method for hindcast, which performs best for PM$_{2.5}$ concentrations, and can also reduce the output of IO files to improve computing efficiency. For forecasting, the method of restart simulation is suggested, which can reach a similar model performance as the continuous simulation. If the restart simulation cannot be used owing to the limitation of computing resources and storage space when forecasting PM$_{2.5}$ concentrations, we attempt to extend the spin-up time as much as possible, at least 27 h according to our results.

Code and data availability

The source codes of the WRF model version 3.9.1.1 used in this study are available online at https://www2.mmm.ucar.edu/wrf/users/download/get_source.html(NCAR, 2020, last access: 4 June 2020). The CAMx version 6.1 code is available at http://www.camx.com/download/default.aspx(ENVIRON, 2020, last access: 4 June 2020), and the SMOKE version 2.4 code is available at https://www.cmascenter.org/smoke/ (CMAS, 2020, last access: 4 June 2020). The global final analysis data (FNL) were obtained from https://rda.ucar.edu/datasets/ds083.2/(NCEP, 2000, last access: 4 June 2020). The dataset related to this manuscript is available online via ZENODO (https://doi.org/10.5281/zenodo.3824676)(Xiao et al., 2020).

Author contribution

Han Xiao conducted the simulation and prepared the materials. Qizhong Wu designed the WRF-SMOKE-CAMx modelling system for Xi'an, including emission processes. Xiaochun Yang collected the local emission inventory in Shaanxi Province and assisted in the emission processes. Lanning Wang and Huaqiong Cheng helped prepare the model dataset and figure.

Acknowledgements

The National Key R&D Program of China (2017YFC0209805), the National Natural Science Foundation of China (41305121), and the Beijing Advanced Innovation Program for Land Surface funded this work.

Appendix A

Statistical parameters for the model evaluation:

Mean bias (MB):

$$\text{MB} = \frac{\sum(M_i - O_i)}{n} \qquad (A1)$$

Mean error (ME):

$$\text{ME} = \frac{\sum |M_i - O_i|}{n} \qquad (A2)$$

410 Normalised mean bias (NMB):

$$\text{NMB} = \frac{\sum (M_i - O_i)}{\sum O_i} \qquad (A3)$$

Normalised mean error (NME):

$$\text{NME} = \frac{\sum |M_i - O_i|}{\sum O_i} \qquad (A4)$$

Root Mean Square Error (RMSE):

415 $$\text{RMSE} = \left[\frac{1}{n} \sum_{i=1}^{n} (M_i - O_i)^2 \right]^{\frac{1}{2}} \qquad (A5)$$

Correlation coefficient (R):

$$R = \frac{\sum_{i=1}^{n}(M_i - \bar{M})(O_i - \bar{O})}{\sqrt{\sum_{i=1}^{n}(M_i - \bar{M})^2 \sum_{i=1}^{N}(O_i - \bar{O})^2}} \qquad (A6)$$

Index of agreement (IOA):

$$\text{IOA} = 1 - \frac{\sum_{i=1}^{n}(M_i - O_i)^2}{\sum_{i=1}^{n}(|M_i - \bar{O}| + |O_i - \bar{O}|)^2} \qquad (A7)$$

420 Normalised Standard Deviations (NSD):

$$\text{NSD} = \frac{\sqrt{\frac{\sum_{i=1}^{n}(M_i - \bar{M})^2}{n}}}{\sqrt{\frac{\sum_{i=1}^{n}(O_i - \bar{O})^2}{n}}} \qquad (A8)$$

In the equations, M_i and O_i represent the simulated value and observation value of a station, respectively. n represents the number of stations. $\bar{M}$ and $\bar{O}$ represent the average values of the simulated and observation values, respectively.

References

425 Appel, K. W., Napelenok, S. L., Foley, K. M., Pye, H. O. T., Hogrefe, C., Luecken, D. J., Bash, J. O., Roselle, S. J., Pleim, J. E., Foroutan, H., Hutzell, W. T., Pouliot, G. A., Sarwar, G., Fahey, K. M., Gantt, B., Gilliam, R. C., Heath, N. K., Kang, D., Mathur, R., Schwede, D. B., Spero, T. L., Wong, D. C., and Young, J. O.: Description and evaluation of the Community Multiscale Air Quality (CMAQ) modeling system version 5.1, Geosci. Model Dev., 10, 1703–1732, https://doi.org/10.5194/gmd-10-1703-2017, 2017.

430 Briggs, G.: Discussions on chimney plumes in neutral and stable surroundings, Atmos. Environ., 6, 507–510, 1972.

Briggs, G.A.: Plume rise and buoyancy effects, Atmospheric Science and Power Production, 327–366, 1984.

Cao, G., Zhang, X., Gong, S., An, X., and Wang, Y.: Emission inventories of primary particles and pollutant gases for China, Chinese Sci. Bull., 56, 781–788, https://doi.org/10.1007/s11434-011-4373-7, 2011.

Cao, J.J., Shen, Z.X., Chow, J.C., Watson, J.G., Lee, S.C., Tie, X.X., Ho, K.F., Wang, G.H., and Han, Y.M.: Winter and summer $PM_{2.5}$ chemical compositions in fourteen Chinese cities, J. Air Waste Manage., 62, 1214–1226, https://doi.org/10.1080/10962247.2012.701193, 2012.

CCCPSC: The Pollution Source Census Data Set (Statistic), Collected Works about the First China Pollution Source Survey Data (V), Compilation Committee of China Pollution Source Census I, China Environment Science Press, Beijing, 228–245, 2011.

Chang, J.S., Brost, R.A., Isaksen, I.S.A., Madronich, S., Middleton, P., Stockwell, W.R., and Walcek, C.J.: A three-dimensional eulerian acid deposition model: physical concepts and formulation, J. Geophys. Res.-Atmos., 92, 14681-14700, https://doi.org/10.1029/JD092iD12p14681, 1987.

Chang, J. and Hanna, S.: Air quality model performance evaluation, Meteorology and Atmospheric Physics, 87, 167-196, https://doi.org/10.1007/s00703-003-0070-7, 2004.

Chen, H. S., Wang, Z. F., Li, J., Tang, X., Ge, B. Z., Wu, X. L., Wild, O., and Carmichael, G. R.: GNAQPMS-Hg v1.0, a global nested atmospheric mercury transport model: model description, evaluation and application to trans-boundary transport of Chinese anthropogenic emissions, Geosci. Model Dev., 8, 2857–2876, https://doi.org/10.5194/gmd-8-2857-2015, 2015.

CMAS: SMOKE version 2.4, available at: https://www.cmascenter.org/smoke/, last access: 4 June, 2020.

Colella, P., and Woodward, P.R.: The Piecewise Parabolic Method (PPM) for Gas-dynamical Simulations, J. Comput. Phys., 54, 174-201, https://doi.org/10.1016/0021-9991(84)90143-8, 1984.

Dobson, J.E., Bright, E.A., Coleman, P.R., Durfee, R.C., and Worley, B.A.: Landscan: a global population database for estimating populations at risk, Photogramm. Eng. Rem. S., 66, 849–857, 2000.

Dudhia, J.: Numerical study of convection observed during the winter monsoon experiment using a mesoscale two-dimensional model, J. Atmos. Sci. 46, 3077-3107, https://doi.org/10.1175/1520-0469(1989)046<3077:NSOCOD>2.0.CO;2, 1989.

Dudhia, J.: A multi-layer soil temperature model for MM5, The Sixth PSU/NCAR Mesoscale Model Users' Workshop, Boulder, Colorado, 1996.

Eder, B., and Yu, S.: A performance evaluation of the 2004 release of Models-3 CMAQ, Atmos. Environ., 40,4811-4824, https://doi.org/10.1016/j.atmosenv.2005.08.045, 2006.

ENVIRON: User Guide for Comprehensive Air Quality Model with Extensions Version 6.0, available at: http://www.camx.com/files/camxusersguide_v6-00.pdf, 2013.

ENVIRON: CAMx version 6.1, available at: http://www.camx.com/download/default.aspx, last access: 4 June 2020.

Gates, W., Boyle, J., Covey, C., Dease, C., Doutriaux, C., Drach, R., Fiorino, M., Gleckler, P., Hnilo, J., Marlais, S., Phillips, T., Potter, G., Santer, B., Sperber, K., Taylor, K., and Williams, D.: An overview of the results of the atmospheric model

465   inter-comparison project, B. Am. Meteorol. Soc., 80, 29–55, https://doi.org/10.1175/1520-0477(1999)080<0029:AOOTRO>2.0.CO;2, 1999.

Gilliam, R. C., Hogrefe, C., Godowitch, J. M., Napelenok, S., Mathur, R., and Rao, S. T.: Impact of inherent meteorology uncertainty on air quality model predictions, J. Geophys. Res.-Atmos., 120, 12259–12280, https://doi.org/10.1002/2015JD023674, 2015.

470   Grell, G.A., Peckham, S. E., Schmitz, R., Mckeen, S. A., Frost, G., Skamarock, W. C., and Eder, B.: Fully coupled "online" chemistry within the WRF model, Atmos. Environ., 39, 6957-6975, https://doi.org/10.1016/j.atmosenv.2005.04.027, 2005.

Hertel O., Berkowics, R., Christensen, J. and Hov, Ø.: Test of two numerical schemes for use in atmospheric transport-chemistry models, Atmos. Environ., 27, 2591-2611, https://doi.org/10.1016/0960-1686(93)90032-T, 1993.

Hong, S.Y., Dudhia, J., and Chen, S.H.: A revised approach to ice microphysical processes for the bulk parameterization of 475   clouds and precipitation, Mon. Weather Rev., 132, 103-120. https://doi.org/10.1175/1520-0493(2004)132<0103:ARATIM>2.0.CO;2, 2004.

Hong, S.Y., Noh, Y., and Dudhia, J.: A new vertical diffusion package with an explicit treatment of entrainment processes, Mon. Weather Rev., 134, 2318-2341, https://doi.org/10.1175/MWR3199.1, 2006.

Houyoux, M. R. and Vukovich, J. M.: Updates to the Sparse Matrix Operator Kernel Emissions (SMOKE) modeling system 480   and integration with Models-3, The Emission Inventory: Regional Strategies for the Future, Air Waste Management Association, Raleigh, N. C., 1461, 1999.

Huang, R. J., Zhang, Y., Bozzetti, C., Ho, K. F., Cao, J., Han, Y., Daellenbach, K., Slowik, J., Platt, S., Canonaco, F., Zotter, P., Wolf, R., Pieber, S., Bruns, E., Crippa, M., Ciarelli, G., Piazzalunga, A., Schwikowski, M., Abbaszade, G., and Prevot, A.: High secondary aerosol contribution to particulate pollution during haze events in China, Nature, 514, 218–222, 485   https://doi.org/10.1038/nature13774, 2014.

Kain, J. S.: The Kain–Fritsch convective parameterization: An update, J. Appl. Meteorol., 43, 170–181, https://doi.org/10.1175/1520-0450(2004)043<0170:TKCPAU>2.0.CO;2, 2004.

Kato N, and Akimoto H.: Anthropogenic emission of SO_2 and NOx in Asia: Emission inventories, Atmos. Environ., 26, 2997–3017, https://doi.org/10.1016/0960-1686(92)90291-R, 1992.

490   Li, L., Chen, C. H., Fu, J. S., Huang, C., Streets, D. G., Huang, H. Y., Zhang, G. F., Wang, Y. J., Jang, C. J., Wang, H. L., Chen, Y. R., and Fu, J. M.: Air quality and emissions in the Yangtze River Delta, China, Atmos. Chem. Phys., 11, 1621-1639, https://doi.org/10.5194/acp-11-1621-2011, 2011.

Li, L., Cheng, S. Y., Li, J. B., Lang, J. L., and Chen, D. S.: Application of MM5-CAMx- PSAT modeling approach for investigating emission source contribution to atmospheric SO_2 pollution in Tangshan, Northern China, Math. Probl. Eng., 495   2013, 1-12, https://doi.org/10.1155/2013/136453, 2013.

Li, X., Zhang, Q., Zhang, Y., Zhang, L., Wang, Y., Zhang, Q., Li, M., Zheng, Y., Geng, G., Wallington, T., Han, W., Shen, W., and He, K.: Attribution of $PM_{2.5}$ exposure in Beijing–Tianjin–Hebei region to emissions: implication to control strategies, Sci. Bull., 62, 957–964, https://doi.org/10.1016/j.scib.2017.06.005, 2017a.

Li C, Mclinden C, Fioletov V, et al.: India Is Overtaking China as the World's Largest Emitter of Anthropogenic Sulfur Dioxide,
Scientific Reports, 7(1), 14304, https://doi.org/10.1038/s41598-017-14639-8, 2017b.

Li, X. B., Liu, H. B., Zhang, Z. Y., and Liu, J. J.: Numerical simulation of an extreme haze pollution event over the North China Plain based on initial and boundary condition ensembles, Atmospheric and Oceanic Science Letters, 12, 434-443, https://doi.org/10.1080/16742834.2019.1671136, 2019.

Long, X., Li, N., Tie, X., Cao, J., Zhao, S., Huang, R., Zhao, M., Li, G., and Feng, T.: Urban dust in the Guanzhong Basin of China, part I: A regional distribution of dust sources retrieved using satellite data, Sci. Total Environ., 541, https://doi.org/10.1016/j.scitotenv.2015.10.063, 1603-1613, 2016.

Mlawer, E. J., Taubman, S. J., Brown, P. D., Iacono, M. J., and Clough, S.A.: Radiative transfer for inhomogeneous atmospheres: RRTM, a validated correlated-k model for the longwave. J. Geophys. Res. Atmos. 102, 16663-16682, https://doi.org/10.1029/97JD00237, 1997.

NCAR: WRF model, available at: https://www2.mmm.ucar.edu/wrf/users/download/get_source.html, last access: 4 June 2020.

National Centers for Environmental Prediction/National Weather Service/NOAA/U.S. Department of Commerce. 2000, updated daily. NCEP FNL Operational Model Global Tropospheric Analyses, continuing from July 1999. Research Data Archive at the National Center for Atmospheric Research, Computational and Information Systems Laboratory. https://doi.org/10.5065/D6M043C6, last access: 4 June 2020.

Nenes, A., Pandis, S.N., and Pilinis, C.: Continued development and testing of a new thermodynamic aerosol module for urban and regional air quality models, Atmos. Environ., 33, 1553-1560, https://doi.org/10.1016/S1352-2310(98)00352-5, 1999.

Ni, T. R., Han, B., and Bai, Z. P.: Source Apportionment of PM_{10} in Four Cities of Northeastern China, Aerosol Air Qual. Res., 12, 571-582, https://doi.org/10.4209/aaqr.2011.12.0243, 2012.

Ohara, T., Akimoto, H., Kurokawa, J., Horii, N., Yamaji, K., Yan, X., and Hayasaka, T.: An Asian emission inventory of anthropogenic emission sources for the period 1980–2020, Atmos. Chem. Phys., 7, 4419–4444, https://doi.org/10.5194/acp-7-4419-2007, 2007.

Panagiotopoulou, A., Charalampidis, P., Fountoukis, C., Pilinis, C., and Pandis, S. N.: Comparison of PMCAMx aerosol optical depth predictions over Europe with AERONET and MODIS measurements, Geosci. Model Dev., 9, 4257–4272, https://doi.org/10.5194/gmd-9-4257-2016, 2016.

Seaman, N. L.: Meteorological modeling for air-quality assessments, Atmos. Environ., 34, 2231–2259, https://doi.org/10.1016/S1352-2310(99)00466-5, 2000.

Seinfeld, J.H., and Pandis, S.N.: Atmospheric Chemistry and Physics, From Air Pollution to Climate Change, John Wiley and Sons, Inc., New York. 1998.

Sistla, G., Zhou, N., Hao, W., Ku, J.-Y., Rao, S. T., Bornstein, R., Freedman, F., and Thunis, P.: Effects of uncertainties in meteorological inputs on Urban Airshed Model predictions and ozone control strategies, Atmos. Environ., 30, 2011–2025, https://doi.org/10.1016/1352-2310(95)00268-5, 1996.

Skamarock, W.C., Klemp, J.B., Dudhia, J., Gill, D. O., Barker, D. M., Duda, M. G., Huang, X. Y., Wang, W., and Powers, J.G.: A Description of the Advanced Research WRF Version3 (No. NCAR/TN-475+STR), University Corporation for Atmospheric Research, https://doi.org/10.5065/D68S4MVH. NCAR, 2008.

535 Streets, D. G., Bond, T. C., Carmichael, G. R., Fernandes, S. D., Fu, Q., He, D., Klimont, Z., Nelson, S. M., Tsai, N. Y., Wang, M. Q., WOO, J. H., and Yarber K. F.: An inventory of gaseous and primary aerosol emissions in Asia in the year 2000, J. Geophys. Res.-Atmos., 108, 8809-8831, https://doi.org/10.1029/2002JD003093, 2003.

Tang, X., Wang, Z. F., Zhu, J., Gbaguidi, A., and Wu, Q. Z.: Ensemble-Based Surface O3 Forecast over Beijing, Climatic and Environmental Research, 15, 677–684, 2010 (in Chinese).

540 Taylor, K.: Summarizing multiple aspects of model performance in a single diagram, J. Geophys. Res.-Atmos., 106, 7183–7192, https://doi.org/10.1029/2000JD900719, 2001.

Wang, H., Chen, H., Wu, Q., Lin, J., Chen, X., Xie, X., Wang, R., Tang, X., and Wang, Z.: GNAQPMS v1.1: accelerating the Global Nested Air Quality Prediction Modeling System (GNAQPMS) on Intel Xeon Phi processors, Geosci. Model Dev., 10, 2891–2904, https://doi.org/10.5194/gmd-10-2891-2017, 2017.

545 Wang, L. T., Zhang, Q., Hao, J. M., and He, K. B.: Anthropogenic CO emission inventory of Mainland China, Acta Scientiae Circumstantiae, 25, 1580–1585, https://doi.org/10.13671/j.hjkxxb.2005.12.002, 2005 (in Chinese).

Wang, P., Cao, J. J., Shen, Z., Han, Y., Lee, S. C., Huang, Y., Zhu, C. S., Wang, Q., Xu, H., Huang, R. J.: Spatial and seasonal variations of PM2.5 mass and species during 2010 in Xi'an, China, Sci. Total Environ., 508, 477-487. https://doi.org/10.1016/j.scitotenv.2014.11.007, 2015.

550 Wang, Z., Xie, F., Wang, X., An, J., and Zhu, J.: Development and application of nested air quality prediction modeling system, Chinese Journal of Atmospheric Science, 30, 778–790, https://doi.org/10.3878/j.issn.1006-9895.2006.05.07, 2006 (in Chinese).

Wu, D., Fung, J. C. H., Yao, T., and Lau, A. K. H.: A study of control policy in the Pearl River Delta region by using the particulate matter source apportionment method, Atmos. Environ., 76, 147-161,

555 https://doi.org/10.1016/j.atmosenv.2012.11.069, 2013.

Wu, Q., Wang, Z., Gbaguidi, A., Tang, X., and Zhou, W.: Numerical study of the effect of traffic restriction on air quality in Beijing, Sola, 6 (Special Edition), 17–20, https://doi.org/10.2151/sola.6A-005, 2010.

Wu, Q. Z., Xu, W. S., Shi, A. J., Li, Y. T., Zhao, X. J., Wang, Z. F., Li, J. X., and Wang, L. N.: Air quality forecast of PM_{10} in Beijing with community multi-scale air quality modeling (CMAQ) system: emission and improvement, Geosci. Model

560 Dev., 7, 2243–2259, https://doi.org/10.5194/gmd-7-2243-2014, 2014.

Xiao, H., Wu, Q., Yang, X., Wang, L., Cheng, H.: The dataset of the manuscript "Numerical study of the initial condition and emission on simulating PM2.5 concentrations in Comprehensive Air Quality Model with extensions version 6.1 (CAMx v6.1): Taking Xi'an as example", Zenodo, https://doi.org/10.5281/zenodo.3824676, 2020.

Xiao, H., Yang, X. C., Wu, Q. Z., Bai, Q. M., Cheng, H. Q., Chen, X. S., Xue, R., Du, M. M., Huang, L., Wang, R. R., and Wang, H.: Estimate emissions of construction fugitive dust in Xi'an, Acta Scientiae Circumstantiae, 39, 222-228, https://doi.org/10.13671/j.hjkxxb.2018.0377, 2019 (in Chinese).

Yang, X., Wu, Q., Zhao, R., Cheng, H., He, H., Ma, Q., Wang, L., and Luo, H.: New method for evaluating winter air quality: $PM_{2.5}$ assessment using Community Multi-Scale Air Quality Modeling (CMAQ) in Xi'an, Atmos. Environ., 211, 18-28, https://doi.org/10.1016/j.atmosenv.2019.04.019, 2019.

Yang, X., Xiao, H., Wu, Q., Wang, L., Guo, Q., Cheng, H., Wang, R., and Tang, Z.: Numerical study of air pollution over a typical basin topography: Source appointment of fine particulate matter during one severe haze in the megacity Xi'an, Sci. Total Environ., 708, 135213, https://doi.org/10.1016/j.scitotenv.2019.135213, 2020.

Yarwood. G., Rao, S., Yocke, M., and Whitten, G. Z.: Updates to the Carbon Bond chemical mechanism: CB05, Final Report prepared for US EPA. Available at: http://www.camx.com/publ/pdfs/CB05_Final_Report_120805.pdf, 2005.

Zhang, L., Brook, J. R., and Vet, R.: A revised parameterization for gaseous dry deposition in air-quality models. Atmos. Chem. Phys., 3, 2067–2082, https://dx.doi.org/10.5194/acp-3-2067-2003, 2003.

Zhang, L., Gong, S., Padro, J., Barrie, L.: A size-segregated particle dry deposition scheme for an atmospheric aerosol module, Atmos. Environ., 35, 549-560, https://doi.org/10.1016/S1352-2310(00)00326-5, 2001.

Zhang, Q., Streets, D. G., Carmichael, G. R., He, K., Huo, H., Kannari, A., Klimont, Z., Park, I., Reddy, S., Fu, J. S., Chen, D., Duan, L., Lei, Y., Wang, L., and Yao, Z.: Asian emissions in 2006 for the NASA INTEX-B mission, Atmos. Chem. and Phys., 9, 5131–5153, https://doi.org/10.5194/acp-9-5131-2009, 2009.

Zhang, Q., Klimont, Z., Streets, D. Huo, H. and He, H.: An anthropogenic PM emission model for China and emission inventory for the year 2001, Progress in Natural Science, 16, 223–231, 2006 (in Chinese).

Zhang, X. Y., Cao, J. J., Li, L. M., Arimoto, R., Cheng, Y., Huebert, B., and Wang, D.: Characterization of atmospheric aerosol over Xi'an in the south margin of the Loess Plateau, China, Atmos. Environ., 36, 4189–4199, https://doi.org/10.1016/S1352-2310(02)00347-3, 2002.

Zhang, Y., Bocquet, M., Mallet, V., Seigneur, C., and Baklanov, A.: Real-Time Air Quality Forecasting, Part I: History, techniques, and current status, Atmos. Environ., 60, 632-655, https://doi.org/10.1016/j.atmosenv.2012.06.031, 2012.

Zhang, Y. P., Li, X., Nie, T., Qi, J., Chen, J., and Wu, Q.: Source apportionment of $PM_{2.5}$, pollution in the central six districts of Beijing, China, J. Clean. Prod., 174, 661-669, https://doi.org/10.1016/j.jclepro.2017.10.332, 2018.